Cerebral Cortex, 2019; 1–16

doi: 10.1093/cercor/bhz054
Original Article

ORIGINAL ARTICLE

Evolution of Brain Connections: Integrating Diffusion MR Tractography With Gene Expression Highlights Increased Corticocortical Projections in Primates

Christine J. Charvet[1], Arthi Palani[2,3], Priya Kabaria[2,4] and Emi Takahashi[2]

[1]Department of Psychology, Delaware State University, Dover, DE 19901, USA, [2]Division of Newborn Medicine, Department of Medicine, Boston Children's Hospital, Harvard Medical School, Boston, MA 02215, USA, [3]Medical Sciences in the College of Arts and Sciences, Boston University, Boston, MA 02215, USA and [4]Department of Behavioral Neuroscience, Northeastern University, Boston, MA 02115, USA

Address correspondence to Christine Charvet, Department of Psychology, Delaware State University, Dover, DE 19901, USA. Email: charvetcj@gmail.com/ Emi Takahashi, Division of Newborn Medicine, Boston Children's Hospital, Harvard Medical School, 401 Park Dr, Boston, MA 02215, USA. Email: Emi.Takahashi@childrens.harvard.edu

Abstract

Diffusion MR tractography permits investigating the 3D structure of cortical pathways as interwoven paths across the entire brain. We use high-resolution scans from diffusion spectrum imaging and high angular resolution diffusion imaging to investigate the evolution of cortical pathways within the euarchontoglire (i.e., primates, rodents) lineage. More specifically, we compare cortical fiber pathways between macaques (*Macaca mulatta*), marmosets (*Callithrix jachus*), and rodents (mice, *Mus musculus*). We integrate these observations with comparative analyses of Neurofilament heavy polypeptide (*NEFH*) expression across the cortex of mice and primates. We chose these species because their phylogenetic position serves to trace the early evolutionary history of the human brain. Our comparative analysis from diffusion MR tractography, cortical white matter scaling, and *NEFH* expression demonstrates that the examined primates deviate from mice in possessing increased long-range cross-cortical projections, many of which course across the anterior to posterior axis of the cortex. Our study shows that integrating gene expression data with diffusion MR data is an effective approach in identifying variation in connectivity patterns between species. The expansion of corticocortical pathways and increased anterior to posterior cortical integration can be traced back to an extension of neurogenetic schedules during development in primates.

Key words: cortex, cortical convolution, diffusion MRI, evolution, primates

Introduction

One of the fundamental issues in evolutionary neuroscience is to understand the principles with which connections evolve (Nudo and Masterton 1988, 1990; Barbas and Rempel-Clower 1997; Striedter 2005; Kaas 2012; Hofman 2014; Barbas 2015; Hilgetag et al. 2016; Horvát et al. 2016; Beul et al. 2017; Das and Takahashi 2017; Goulas et al. 2018). Diffusion MR imaging has begun to answer long-standing questions in the field of evolutionary neurobiology (Rilling et al. 2008; Takahashi et al. 2011; Charvet, Hof et al. 2017; Das and Takahashi 2017; Mortazavi et al. 2017). For instance, diffusion MR tractography has demonstrated that the human arcuate fasciculus is expanded relative to that of other primates, which might have been an important pathway responsible for the emergence of language in humans (Rilling et al. 2008; Rilling 2014). More recently, the use of diffusion MR tractography has demonstrated that primates possess increased anterior to posterior cortical integration compared with a number of other mammals (Charvet, Hof et al. 2017). We

use diffusion MR tractography to investigate the evolutionary history of cortical pathways across euarchontoglires (i.e., primates, rodents) to trace the early evolutionary history of the primate lineage leading to the human brain.

Diffusion MR imaging is a high-throughput and noninvasive method that is instrumental in investigating long-range projection pathways coursing across the white matter of the brain. Questions focused on the evolution of connections have traditionally been addressed with tract-tracers, which are time-consuming, invasive, and unavailable to the study of the human brain (Gilbert and Kelly 1975; Kennedy and Bullier 1985; Barbas 1986; Nudo and Masterton 1990; Hof et al. 1995). We here integrate observations from diffusion MR tractography with comparative analyses of gene expression data from bulk and single cells to trace the evolution of cortical pathways in euarchontoglires. We focus especially on species differences in the expression of Neurofilament heavy polypeptide (*NEFH*) because *NEFH* is preferentially expressed by large neurons with long axons projecting over long distances (Hof et al. 1995; Marszalek et al. 1996; Friedland et al. 2006; Nguyen et al. 2017). Therefore, comparative analyses of *NEFH* expression levels coupled with observations from diffusion MR tractography can be used to identify evolutionary changes in long-range projection patterns (Hof et al. 1995).

The location of a neuronal soma across the depth of the cortex predicts projection patterns to some extent. Variation in neuron numbers across the depth of the cortex can identify evolutionary changes in connectivity patterns. Although little is known about the extent to which these stereotypical projection patterns vary across species, neurons located superficial to the cortical surface (i.e., upper layer neurons, layers II–IV) preferentially project cross-cortically. Layer IV neurons are local circuit neurons. This is in contrast with neurons located towards the white matter (i.e., lower layer neurons, layers V–VI) that preferentially, though not exclusively, project subcortically (Gilbert and Kelly 1975; Kennedy and Bullier 1985; Barbas 1986; Nudo and Masterton 1990). That is, some layer V neurons may form long-range, short-range, or collosal pathways (Barbas 1986; Barbas and Rempel-Clower 1997; Barbas, Hilgetag et al. 2005; Barbas, Medalla et al. 2005; Hilgetag and Grant 2010). Primates possess disproportionately more layers II–IV neurons compared with many other mammals, including rodents (Charvet et al. 2015; Charvet, Hof et al. 2017; Charvet, Šimić et al. 2017; Charvet, Stimpson et al. 2017). Although the relative contribution of layer II–III versus layer IV neuron numbers has not been systematically quantified across the cortex of different species, the observation that primate cortices possess an expansion of layer II–IV neuron numbers suggests that primates may possess increased cross-cortically projecting neurons compared with rodents. However, it remains unclear whether the increase in upper layer neuron numbers in primates is concomitant with increased long-ranging cortical projections, local circuit neurons, or both. Tract-tracing studies and diffusion MR studies have reported that primates possess a large number of long-range cross-cortically projecting neurons across the anterior to posterior axes of the cortical white matter (Schmahmann et al. 2007; Schmahmann and Pandya 2009; Charvet, Hof et al. 2017). Given these reports, the aim of the present study is to test whether primates do indeed possess more long-range cross-cortically projecting neurons compared with other species such as mice.

We integrate comparative analyses of *NEFH* expression with diffusion MR tractography to test for deviations in long-range cortically projecting neurons in primates and in rodents. We select to compare brain fiber pathways between macaque (*Macaca mulatta*, Pandya and Kuypers 1969; Schmahmann et al. 2007; Schmahmann and Pandya 2009), marmoset (*Callithrix jacchus*, Okano and Mitra 2015), and mice (*Mus musculus*, Wu et al. 2013), in part, because brain pathways have been mapped in earlier studies with the use of tract-tracers and MRI diffusion tractography in these species. We also select these species because of their phylogenetic position. Rodents (e.g., mice) are the closest living-outgroup to primates and marmosets are phylogenetically intermediate between macaques and rodents (Bininda-Emonds et al. 2007; Perelman et al. 2011). Comparative analyses of pathways between rodents and primates serve to trace the early evolutionary history of the human brain.

The main finding from the present analysis is that there are major modifications to cortical pathways between primates and mice. Integrating comparative analyses from diffusion MR tractography and *NEFH* expression patterns demonstrate that primates possess an expansion in long-range corticocortical pathways compared with mice. Many of the identified cortico-cortical long-range projection pathways course across the anterior to posterior axes of the cortex, suggesting that the primate cortex deviates from other species in possessing increased anterior to posterior cross-cortical integration.

Materials and Methods

Specimen Preparation

Brains of species used for the present study were collected opportunistically from a group involved in vision research at Harvard Medical School (HMS). All procedures were approved by the Institutional Review Board (IRB) at Massachusetts General Hospital and HMS where our MRI scans were performed. No animals were killed for the purpose of this study. We used brains of 4 adult macaques, 3 marmoset monkeys, and 4 mice. Briefly, the brains of macaques, marmosets, and mice were perfused with phosphate-buffered saline solution followed by 4% paraformaldehyde, and fixed for 1 week in 4% paraformaldehyde solution containing 1 mM gadolinium (Gd-DTPA) MRI contrast agent to reduce the T1 relaxation time while ensuring that enough T2-weighted signal remained. For MR image acquisition, the brains were placed in a Fomblin solution (Fomblin Profludropolyether; Ausimont). Specimens were scanned with a 4.7 T Bruker Biospec MR system at the A. A. Martinos Center for Biomedical Imaging. The brains of 2 human adults without neurologic disease were selected from autopsies. The autopsies were performed with consent of the family and included permission for research under our IRB-approved protocol.

Scanning Parameters

For all scans, we determined the highest spatial resolution for each specimen with an acceptable signal-to-noise ratio of more than 130. For mice and marmosets, the pulse sequence used for image acquisition was a 3D diffusion-weighted spin-echo echo-planar imaging sequence at a 4.7 T Bruker Biospec MR system with a high-performance gradient and a radio-frequency coil that better fits the small brains. We used TR 400 ms, TE 20 ms, with number of segments 2. Spatial resolution was 0.13 × 0.13 × 0.17 mm^3 for mice, and 0.23 × 0.23 × 0.28 mm^3 for marmoset. A total of 60 diffusion-weighted measurements (b = 4000 sec/mm^2) and 1 nondiffusion-weighted (b = 0) measurement were acquired, with δ = 12.0 msec, Δ = 24.0 ms as previously described (Fame

et al. 2016; Kanamaru et al. 2017). The total acquisition time was about 2 h and 10 min for each imaging session.

Human brains were scanned on a 3-Tesla TimTrio MRI scanner (Siemens Medical Solutions, Erlangen, Germany) using a 32-channel head coil. Diffusion data were acquired using a 3D diffusion-weighted steady-state free-precession sequence (McNab et al. 2009) that used 44 diffusion-weighted measurements. Spatial resolution was $1.0 \times 1.0 \times 1.0\,mm^3$. Total scan time for each specimen was 5.5 h. Additional diffusion sequence parameters have been previously reported (Edlow et al. 2012; Kolasinski et al. 2013).

We performed diffusion spectrum encoding as previously described for macaques (Wedeen et al. 2005). Briefly, we acquired 515 diffusion-weighted measurements, corresponding to a cubic lattice in q-space contained within the interior of a ball of maximum radius bmax = $4 \times 10^4\,cm^2/s$, with $\delta = 12.0$ ms, $\Delta = 24.2$ ms. The total acquisition time was 18.5 hours for each experiment. Spatial resolution was $0.55 \times 0.55 \times 0.75\,mm^3$. The total acquisition time was about 18 hours. Some of these scans were used in a previous study (Charvet, Hof et al. 2017).

Diffusion Data Analyses—Tractography

We used Diffusion Toolkit to utilize a streamline algorithm for diffusion tractography. Trajectories were propagated by consistently pursuing the orientation vector of least curvature. We terminated tracking when the angle between 2 consecutive orientation vectors was greater than the given threshold (45°) or when the fibers extended outside the brain surface, by using mask images of the brains created by TrackVis (http://trackvis.org) for each specimen. In many tractography studies, FA values are used to terminate fibers in the gray matter, which in adults has lower FA values than the white matter. As one of the objectives of our study was to detect fibers in low FA areas, we used brain mask volumes to terminate tractography fibers without using the FA threshold for tractography, which is an approach consistent with that of previous studies (Takahashi et al. 2010, 2012). Trajectories were displayed on a 3D workstation of TrackVis. The color-coding of fibers is based on a standard RGB code, applied to the vector between the end-points of each fiber (Fig. 1).

Diffusion Data Analyses—ROI Placement and Restriction Parameters

In Trackvis, we used frames set through the hemisphere with a minimum length threshold of 10–15 mm in primates and 5 mm in mice to highlight cortical pathways (Fig. 1), This approach offers a global perspective with which to examine pathways across the brain of different species. We also include a diffusion MR scan of a human brain. Details of procedures for data acquisition have been published previously (Charvet, Hof et al. 2017).

Using ITK-SNAP (http://www.itksnap.org/), we were able to segment the 3D images of each of the brains respectively in order to create a visual representation of the cortical surfaces. We then used TrackVis in order to visualize diffusion tractography pathways and associated diffusion-weighted images as an anatomical reference. Regions of interest (ROIs) were created for each gyrus and associated sulcus. In both macaques and marmosets, multiple spherical ROIs were used for the orbitofrontal, superior temporal and temporal gyri and sulci, and hand-drawn ROIs were used for the calcarine gyrus and sulcus due to the complex structure and depth of the sulcus in the macaque. We did not use length thresholds to identify these pathways.

In order to compare the cingulum bundle, fornix, and thalamocortical/corticothalamic pathways across all 3 species, ROIs were placed following the method previously published (Catani and de Schotten 2008; Song et al. 2015; Cohen et al. 2016). The selected fibers were further filtered for their length with the software program TrackVis. Minimum length thresholds of 58, 15, and 13 mm were utilized for macaques, marmosets, and mice, respectively. In marmosets, a minimum threshold of 15 mm was used in order to isolate pathways of interest. What may constitute equivalent length thresholds between species may be debatable, considering that the brains of the examined species vary in size and length of pathways.

We confirmed our mouse tractography results with tract tracer studies available in the Allen Brain Atlas (http://portal.brain-map.org/; Supplementary Fig. S1). Tract-tracer data are from the Allen Brain Atlas (ABA) mouse brain connectome, which is one of the most comprehensive data-sets to map mouse brain connectivity, from anterograde viral neuronal tracer injections in the wild-type C57BL/6 mouse brain (Oh et al. 2014). We use these data to ensure the concordance of diffusion MR tractography with tractographies from tract-tracers. Injection sites in the Allen Brain Atlas that most closely identify the cingulum bundle (A), fornix (B), thalamocortical (C), and callosal (D) pathways were selected, and ROIs (1 mm in radius) for tractography were placed in the injection sites; the dorsal anterior cingulate cortex (Supplementary Fig. S1A) the hippocampal C1 region (Supplementary Fig. S1B), and the reticlular nucleus of the thalamus (Supplementary Fig. S1C), which were corresponding ROI regions for the images from the Allen Brain Atlas (Supplementary Fig. S1, upper rows).

Comparative Analyses of *NEFH* Expression

Our comparative analysis from diffusion MR tractography suggests that the cortex of primates possess alterations in cross-cortically projecting pathways compared with mice (see also Charvet, Hof et al. 2017). To validate these observations quantitatively, we compare the expression of *NEFH* in primates and mice. *NEFH* is preferentially expressed by neurons with thick myelinated and long axons with high conduction velocities (Marszalek et al. 1996; Usoskin et al. 2015). Thus, *NEFH* can be used to assess species differences in cortical long-range projection patterns (Hof et al. 1995; Friedland et al. 2006; Nguyen et al. 2017). However, it is unclear whether the observed species differences in *NEFH* mRNA expression would reflect differences in NEFH protein expression. Further studies are required to assess whether the observed differences in *NEFH* mRNA entail species differences in NEFH protein expression (Vogel and Marcotte 2012).

We test whether *NEFH* is differentially expressed in the prefrontal and visual cortices of mice ($n = 5$; postnatal day 56) and primates (macaques $n = 5$; 9–21 years of age; chimpanzees $n = 6$, 21–42 years of age; humans, $n = 5$, 21–59 years of age; GEO accession number: GSE49379, Bozek et al. 2014). *NEFH* expression values for humans, chimpanzees, macaques, and mice are in reads per kilobase million (RPKM). Only reads in coding regions, which could be lifted over (with the liftOver tool) across species were considered. Gene expression was quantified as the number of reads aligned to the gene exons divided by the length of the gene exon. To correct for variation in library size across samples, the mean number of reads across all collected samples were divided by the number of reads from the sample of interest.

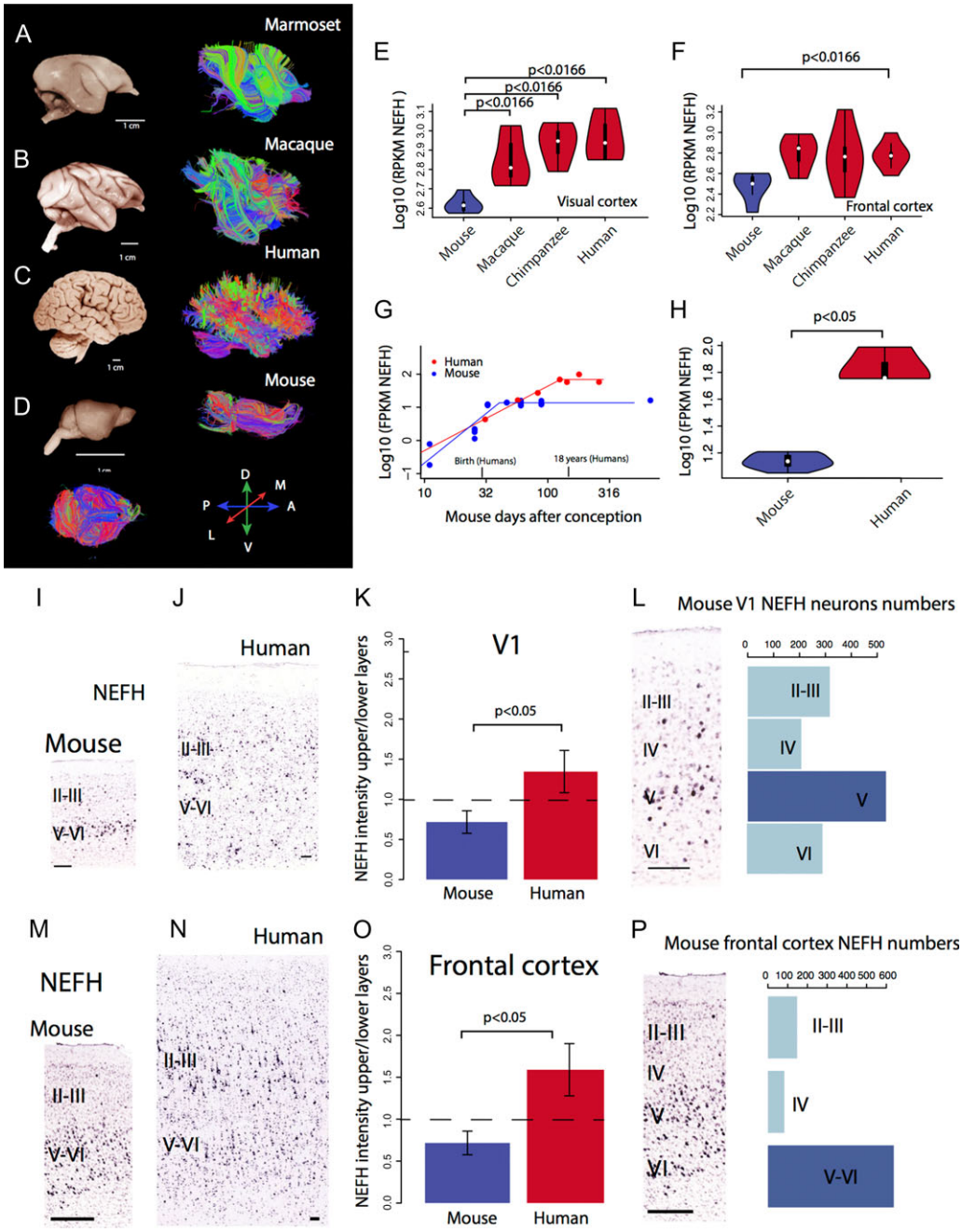

Figure 1. Brain pictures and overall tractography pathways of marmosets (*A*), macaques (*B*), humans (*C*), and mice (*D*). For tractograpy, axial filters were set through the middle of the brain at the level of the thalami. Tractography of marmosets (*A*), macaques (*B*), and humans (*C*) show a number of pathways coursing across various directions through the cortex. In contrast, mice (*D*) possess pathways nearly exclusively coursing across the anterior to posterior axis or the medial to lateral axis. We compare *NEFH* expression values because it is a marker of long-range connecting cortical neurons (Hof et al. 1995). (*E*, *F*) A box plot highlighting the median (white dot), quantiles, and confidence intervals overlaid on a violin plot (i.e., density plot) show the distribution of *NEFH* expression across individuals for each species in the visual cortex (*E*) and the frontal cortex (*F*). *NEFH* expression is significantly higher in the visual cortex (*E*) of humans, chimpanzees, macaques compared with mice. A similar situation is observed in the frontal cortex (*F*) where *NEFH* expression is significantly increased in humans compared with mice. (*G*) Developmental time course of *NEFH* expression shows major differences in *NEFH* expression between humans and mice. *NEFH* expression is plotted against equivalent developmental time points in humans and mice on the axis where age of mice is mapped onto humans (Workman et al. 2013). (*H*) *NEFH* expression increases and reaches a plateau in humans and in mice but the plateau in *NEFH* expression is reached much later than expected in humans after controlling for overall changes in developmental schedules. (*H*) Data from (*G*) shows that *NEFH* expression is significantly greater in humans compared with mice once *NEFH* expression reaches a plateau. (*I*, *J*) *NEFH* mRNA expression is more superficially expressed in humans at 17 years of age compared with mice at postnatal day 56. (*K*) The density of *NEFH* found in upper relative to that observed in lower layers in the primary visual cortex of humans (17–57 years old) is significantly greater in humans than in mice (postnatal day 28–24 months old). (*L*) Single cell RNA sequencing from the mouse primary visual cortex show that there are relatively fewer expressed *NEFH*-labeled cells in upper versus lower layers. These observations are consistent with the notion that *NEFH* expression is much lower in upper layers relative to lower layers in mice. A similar situation is observed in the frontal cortex (*M*–*P*) where *NEFH* is relatively increased in upper versus lower layers in humans (aged 28 years old) relative to mice (P56; *M*–*O*). (*P*) Single cell RNA sequencing analyses with dropviz (http://dropviz.org/) highlights that most of the *NEFH*-labeled neurons are located in lower layers. Abbreviations: A: anterior; P: posterior; M: medial; L: lateral, D: dorsal; V: ventral; FPKM: fragments per kilobase million. (*I*, *J*) Sections of *NEFH* mRNA expression are from the Allen brain atlas 2010 Allen Institute for Brain Science. Allen Human Brain Atlas. Available from: human.brain-map.org. Scale bar: 100 μm.

Although *NEFH* has not been compared quantitatively between primates and rodents, there are qualitative differences in *NEFH* expression across the depth of the cortex between humans and mice (Zeng et al. 2012). However, Zeng et al. 2012 focused exclusively on the primary visual cortex of humans and mice, and it is not clear whether species differences in *NEFH* expression are restricted to the primary visual cortex, or whether these differences in *NEFH* expression span cortical areas other than the primary visual cortex. In primates, *NEFH* expression appears preferentially expressed in upper layers in some cortical areas but not in others (Barbas and García-Cabezas 2016).

For each species, we performed a principal component analysis on the log-based RPKM values of orthologous and expressed genes across the 4 species under study in order to detect and remove outliers. The removal of an outlier was based on whether a sample deviated from most other samples on principal components 1 and 2. We removed a total of 5 outliers from all samples from the prefrontal and visual cortices. We used a Kolmogorov–Smirnov test (ks test) or a t test to explore differences in *NEFH* expression between species. We selected a ks test when the data are not normally distributed, and we used a t test when the data are normally distributed. We tested for equal variance between samples with the var.test function in R.

To investigate potential species differences in developmental trajectories of *NEFH*, we use a previously published RNA sequencing dataset from bulk samples of the frontal cortex of humans (mid-frontal gyrus; $n = 7$) from around birth to 55 years of age and mice from embryonic day 11 to 22 months of age (frontal cortex; $n = 21$; Lister et al. 2013). *NEFH* expression values for both mice and humans are in fragments per kilobase million (FPKM; GEO accession number: GSE47966; Lister et al. 2013). We report boxplots overlaid on density plots (i.e., violin plots) to compare the distribution of *NEFH* expression across species (Fig. 1). We use a model that relies on the timing of transformations across mammalian species to find equivalent stages of development between model organisms and humans (Workman et al. 2013). A total of 271 developmental transformations were acquired across 18 mammalian species (e.g., mice, rats, rhesus macaques, humans). Developmental transformations capture rapid changes that occur during brain development. Many of these developmental transformations focus on changes in synaptogenesis, neuron production, as well myelination. The timing of developmental events can be used to identify corresponding ages across species. To that end, the timing of development transformations (logged-transformed) are regressed against an event scale in each species. The "event scale" is a multivariate measure of overall maturational state of the nervous system, with the generation of the first neurons near "0," with "1" corresponding to about 2 years postnatal in humans. We can use these data to identify whether select developmental processes occur unusually early or late in a given species after controlling for overall changes in developmental schedules (Clancy et al. 2001; Dyer et al. 2009; Charvet, Šimić et al. 2017; Charvet and Finlay 2018, see Supplementary Figs S2 and S3). Because the translating time model extends up to 2 years of age in humans and its equivalent in mice, we extrapolate corresponding ages at later time points. We identified equivalent ages from a linear regression of the logged-based 10 values of days after conception for humans and mice. This permitted extrapolating corresponding ages between the 2 species throughout adulthood in the 2 species (Fig. 1, Supplementary Fig. S3). We identified when *NEFH* expression reaches a linear plateau with the library package easynls (model 3) in R.

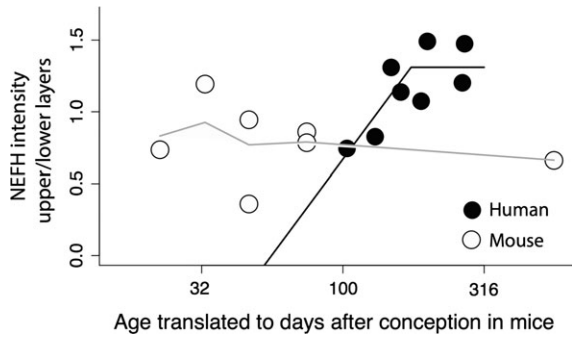

Figure 2. Developmental trajectories in the relative expression of *NEFH* expression in upper versus lower layers in the frontal cortical areas of humans and in mice, respectively. Ages of humans are translated to mice according to the translating time model (see Supplementary Fig. S2). These data show that the relative expression of *NEFH* across layers steadily increases up to about 20 years of age in humans (~5–6 months old mouse) and plateaus between 20 and 28 years of age. The expression of *NEFH* expression steadily increases in upper layers in humans but the expression of *NEFH* in upper versus lower layers remains relatively stable in mice. Testing for a linear plateau with easynls (R library packages) shows that the expression of *NEFH* in upper versus lower layers versus age is significant for a linear plateau ($P < 0.05$; $R^2 = 0.64$) in humans. In mice, the expression of *NEFH* in upper versus lower layers remains relatively stable throughout the examined ages. The relative expression of *NEFH* does not reach a plateau in mice ($P > 0.05$). A smooth spline fit through the data suggests that *NEFH* expression in upper versus lower layers may peak at around postnatal day14 in mice but the relative expression of *NEFH* remains relatively stable while the relative expression of *NEFH* steadily increases in humans. Taken together, these data highlight important heterochronic shifts in *NEFH* expression across layers in both species. These data are consistent with those shown in Figure 1G.

Comparative Analyses of *NEFH* Expression Across Layers

A selective increase in *NEFH* expression in upper layers of the cortex would imply modifications to corticocortical pathways because layer II–III neurons preferentially form corticocortical pathways (Gilbert and Kelly 1975; Kennedy and Bullier 1985; Barbas 1986; Nudo and Masterton 1990; Hof et al. 1995). To test the hypothesis that primates possess evolutionary changes in long-range corticocortical pathways relative to mice, we quantified differences in the relative expression of *NEFH* between upper (layers II–IV) versus lower layers (layers V–VI) in the primary visual cortex and frontal cortical areas of humans and mice (Figs 1 and 2). We reasoned that there were sufficient individuals to identify significant differences in *NEFH* expression between the frontal and visual cortex of humans and mice (Table S1). We also test whether *NEFH* expression is preferentially expressed in upper versus lower layers across the isocortex of mice (rather than select cortical areas; Supplementary Fig. S4). Age and samples used are listed in Table S1. We quantified the density of *NEFH* mRNA expression levels from sections in upper and lower layers of the primary visual cortex and frontal cortical areas of humans and mice. When comparing the relative intensity of *NEFH* expression in upper versus lower layers of adult brains (Fig. 1K,O), we selected to compare *NEFH* expression densities in the primary visual cortex in humans between 8 and 41 years of age and mice between postnatal day 56 to 4 months of age (Table S2). We also selected to compare *NEFH* expression densities in frontal cortical areas in

humans between 17 and 57 years of age and in mice from postnatal day 28 to 24 months of age. As these ages, *NEFH* expression diverges in its pattern of expression between the 2 species (Fig. 1G). We also compare temporal changes in *NEFH* expression between upper and lower layers across humans and mice (Fig. 2). Although we here focus on comparing *NEFH* mRNA expression across cortical layers of humans and mice, the NEFH protein is also expressed in the cortex of mice and primates (i.e., macaques, Supplementary Fig. S5; see Campbell and Morrison 1989). Consistent with comparative analyses of *NEFH* mRNA, it also appears that *NEFH* may be more strongly expressed in upper layers in the frontal cortex of macaques relative to mice (Supplementary Fig. S5).

To quantify differences in *NEFH* mRNA expression, we downloaded images of *NEFH* mRNA labeled sections made available by the Allen Brain Atlas. We placed a rectangular grid through sections that span the 2 cortical areas of interest (i.e., primary visual cortex, frontal cortical areas). We use this grid to randomly select sites along the cortical surface to measure the density in the relative expression levels of *NEFH* in upper and lower layers in the 2 species. Randomly selected frames were aligned along the cortical surface. Frame widths were 500 and 1000 μm in mice and humans, respectively. The height of frames varied with the thickness of upper and lower layers. These analyses were performed in Image J. We used cytoarchitecture from adjacent Nissl-stained section in humans, and in mice, as well as atlases to define cortical areas, as well as upper (i.e., layers II–IV) and lower layers (i.e., layers V–VI). Upper layers were distinguished from lower layers based on a small cell-dense layer IV evident from Nissl-stained sections. This approach is similar to that used previously to quantify upper and lower layer neuron numbers in primates and rodents (Charvet et al. 2015; Charvet, Hof et al. 2017; Charvet, Stimpson et al. 2017).

To compute the relative density of *NEFH* expression in upper versus lower layers in humans and in mice, we binarized images of *NEFH* mRNA expression made available from the Allen Brain Atlas. After images were binarized, we quantified the area occupied by *NEFH*, and the background (i.e., the area not occupied by *NEFH*) in either upper or lower layers separately (Fig. 1G). Dividing the area occupied by *NEFH* with the area occupied by the background corrects for variation in cortical height between samples. We subsequently quantified the ratio of *NEFH* mRNA across layers by dividing the relative area occupied by *NEFH* in upper versus the relative area occupied by *NEFH* in lower layers. Accordingly, a value less than 1 implies that *NEFH* is preferentially expressed in lower layers whereas a value in relative expression above 1 implies that *NEFH* expression is relatively increased in upper layers. We, then, averaged *NEFH* relative intensity values for each specimen, and tested for significant differences in *NEFH* expression between species with the use of a t test (Table S1). We used 4–12 frames per specimen and 2–6 sections per specimen to measure the relative densities in *NEFH* expression in upper and lower layers. To ensure the validity of our results, we used single cell RNA sequencing dataset extracted from the mouse primary visual cortex aged 6–8 weeks of age, as well as those obtained from the frontal cortex (see Supplementary Fig. S6). We computed the number of *NEFH*+ cells across layers of the mouse primary visual cortex or the frontal cortex (Fig. 1L,O). Data acquisition and cell type assignment of primary visual cortex neurons are described in detail and follow that of Hrvatin et al. 2018 (GSE102827). Data acquisition and cell type assignment of frontal cortex neurons are described in detail in Saunders et al. 2018 (GSE116470). Cell type assignments from Saunders et al. 2018 are shown in Supplementary Figure S6.

White Matter Scaling in Primates Versus Rodents and Rabbits

Comparative analyses of cortical white matter volume can be used as an indirect means to identify species differences in long-range corticocortical projections. Axons of neurons forming long distance corticocortical connections course through the cortical white matter. If primates possess more long-range corticocortical projecting neurons, the primate brain may be preferentially composed of cortical white matter compared with rodents. Importantly, the relationship between cortical white matter and overall brain volume varies with brain size such that bigger brains are preferentially composed of cortical white matter than small-brained species (Zhang and Sejnowski 2000). To assess whether the cortical white matter is enlarged in primates versus rodents after controlling for brain size, we measured the volume of the isocortical white matter and the overall brain in small-brained primates (e.g., pygmy marmosets) and large-brained lagomorphs (i.e, rodents, rabbits). Supplementary Table S3 lists sources of MR scans, atlases, and brain weight measurements used for these analyses (Wilber and Gilchrist 1965; Manocha 1979; Bons et al. 1998; Steele 1998; Muñoz-Moreno et al. 2013; Radtke-Schuller et al. 2016; Schilling, Gao, Janve et al. 2017; Schilling, Gao, Stepniewska et al. 2017; Nadkarni et al. 2018; Sakai et al. 2018; Woodward et al. 2018). To measure the cortical white matter and brain volume, we measured the area from a minimum of 5 slices through the brain or the cortical white matter, and multiplied the areas by the slice thickness and spacing to reconstruct volumes. Volumetric measurements were made with image J. Brains may shrink to various degrees depending on fixatives or processing methods used (Striedter and Charvet 2008), and these brains originate from various sources. We therefore used previously reported fresh brain weights and estimate the cortical white matter volume by multiplying the volume of cortical white matter to overall brain volume with reported previously reported brain weights with the exception of the rabbit brain (see Supplementary Table S3). Such an approach corrects for shrinkage of brains that may occur as a result of different fixatives used. The rabbit brain weight by multiplying the volume by 1.036 as a measure of brain weight (Striedter and Charvet 2008; Muñoz-Moreno et al. 2013).

Because standard statistical analyses do not consider that species are not statistically independent of each other, we used phylogeny-generalized-least-squares statistics (PGLS) to obtain phylogenetically controlled slopes of cortical white matter volume regressed against brain weight (Pagel 1999; Freckleton et al. 2000). We test whether taxonomy (i.e, primate vs. lagomorph) accounts for a significant percentage of the variation in cortical white matter volume. These phylogenetically controlled generalized linear models were performed via restricted estimated maximum likelihood with the software program R, and the library package ape. The phylogeny, which includes branch lengths for these species was taken from Bininda-Emonds et al. (2007) (Fig. 3). Regression parameters were found by maximum likelihood estimates (ML). We also report λ, which varies between 0 and 1. A value of 1 indicates that traits covary according to their shared evolutionary history, whereas a value of 0 indicates that the data do not possess a phylogenetic structure (Pagel 1999; Freckleton et al. 2000).

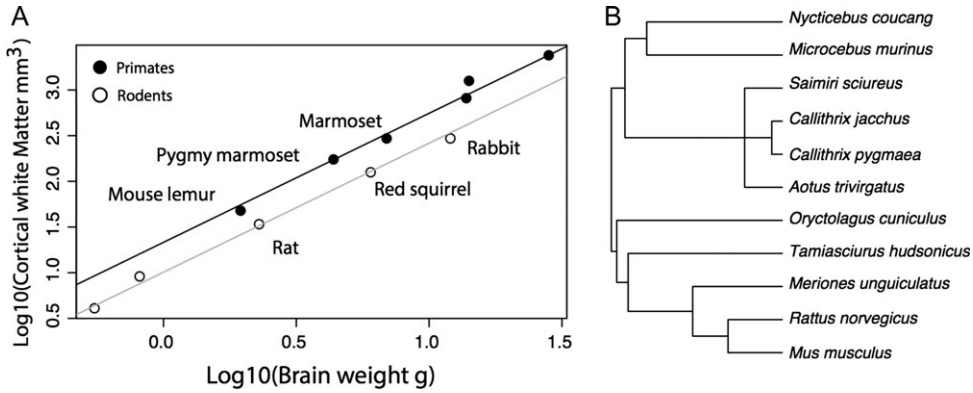

Figure 3. (*A*) The logged-based 10 values of cortical white matter volume in mm^3 are plotted against the logged-based 10 of brain weight in grams (g) in primates (closed circles) and in lagomorphs (rabbits and rodents open circles). Regressions are from a PGLS model with brain size and taxonomy as independent variables and cortical white matter volume as the dependent variable. These data show that, for a given brain size, primates possess disproportionately more cortical white matter volume compared with rodents and rabbits. (*B*) The phylogeny of species used for the PGLS model shown in (*A*).

Results

Overall fiber organization

We use high-resolution diffusion MR tractography to detect fiber pathways coursing across the brain of macaques, humans, marmosets, and mice. These tractographies show interwoven cortical white matter fibers coursing in different directions as assessed from the RGB code applied to the vector of fibers through the cortex of marmoset, macaques, human, and to a lesser extent in mice (Fig. 1A). Axial slice filters set though the cortex of these 3 species highlights a number of pathways coursing across the anterior to posterior and medial to lateral axis of the marmoset, macaque, and human cortex (Fig. 1A–D). The macaque cortex appears to have many more interwoven cortical pathways than the marmoset. A similar situation is observed in the human brain where a large number of pathways are observed coursing in a number of directions through the white matter of the cortex. In other words, the examined primate species possess a multitude of fibers according to the standard (red, green, blue) RGB code, applied to the vector to the direction of pathways. In mice, only the fiber (i.e., cingulate bundle) and pathways coursing in lateral inferior regions are observed coursing across the anterior to posterior of the isocortex (Fig. 1D). A few fibers are also observed coursing principally across the medial to lateral axes of the cortex. At least some, if not most, of these fibers likely comprise the corpus callosum (Fig. 1D). The observation that macaques, marmosets, and humans appear to possess many more multi-dimensional pathways coursing across the axes of the cortex compared with mice led us to test whether there are species differences in long-range connection patterns between some of these species.

An increase in long-range corticocortical projecting neurons or pathways implies primate brains may be preferentially composed of cortical white matter compared with rodents because cortical neurons with long distance targets course through the white matter. We compare cortical white matter volume in small-brained primates (e.g., mouse lemur, pygmy marmoset), and large-brained lagomorphs (e.g., red squirrel, rabbits). Such an approach permits identifying whether primates possess more cortical white matter while controlling for brain size (Zhang and Sejnowski 2000). After controlling for variation in brain size, all examined primates possess disproportionately more cortical white matter than lagomorphs (Fig. 3). For instance, the mouse lemur has disproportionately more cortical white matter than the rat although their brains are similar in size. We use a PGLS model with brain size as the independent variable and cortical white matter volume as the dependent variable. We compare AIC scores from models that include or exclude taxonomy as an independent variable to identify which of the 2 models yields a better fit of the data. A PGLS model with brain size and taxonomy are both significant independent variables accounting for 99% of the variance in cortical white matter volume ($F = 831.1$; $R^2 = 0.99$; $P = 5.264e\text{-}10$; $\lambda = 0$; Fig. 3) and an AIC score of −25.64. A PGLS model that uses brain size alone to predict cortical white matter volume only accounts for 97% of the variance ($F = 339.1$; $P = 1.88e\text{-}08$, $0 < \lambda = 0.1 < 1$, $\lambda = 0$: $P > 0.05$; $\lambda = 1$:$P < 0.05$), with an AIC score model of −8.86. The addition of taxonomy as an independent variable in the PGLS model results in a lower AIC score than one model without taxonomy as an independent variable. These findings demonstrate that primates deviate from rodents in possessing more cortical white matter volume than lagomorphs after controlling for brain size. We next compare gene expression across layers to identify differences in long-range corticocortical projections between primates and rodents.

NEFH is one of the few markers that can be used to detect neurons with thick and long-range axons (Hof et al. 1995), and quantitative comparisons of *NEFH* expression may be instrumental in identifying whether there are differences in long-range corticocortical pathways in primates versus rodents. We compare *NEFH* expression levels between the frontal and the visual cortex of primates and mice. We use a bonferroni significance threshold since we compare 3 primate species with mice. This correction sets our significance threshold to $P < 0.0166$. In the primary visual cortex, the normalized log-based *NEFH* expression values are significantly higher in macaques ($x = 2.85$, SD = 0.12, ks test: $P < 0.0166$, $n = 6$), chimpanzees ($x = 2.93$, SD = 0.10, $n = 5$, ks test: $P < 0.0166$), and humans ($x = 2.96$, SD = 0.12, $n = 5$, ks test: $P < 0.0166$; Fig. 1) compared with mice ($x = 2.93$, SD = 0.10, $n = 5$, Fig. 1E). In the prefrontal cortex, the normalized log-based *NEFH* expression levels are higher in all 3 observed primate species relative to mice we only observed significant differences between the prefrontal cortex of humans versus mice. In the prefrontal cortex, *NEFH* expression is significantly higher in humans ($x = 2.77$, SD = 0.13, $n = 6$, $P < 0.0166$; *t* test, Fig. 1F), but not significantly higher in macaques ($x = 2.48$, SD = 0.15; $P > 0.0166$, $n = 5$, *t* test), and chimpanzees ($x = 2.76$, SD = 0.29, $n = 6$, ks test $P = 0.108$) compared with mice ($x = 2.48$, SD = 0.15, $n = 5$). The finding that *NEFH* expression values are greater in

primates than in mice suggests major changes in long-range cortically projecting neurons between the 2 taxonomic groups.

To further validate the observed increases in *NEFH* expression between primates and mice, we investigate the developmental trajectories of *NEFH* expression levels in the frontal cortex of humans and mice. We rely on the timing of developmental transformations to find corresponding time points between model organisms and humans (Workman et al. 2013). Such an approach permits controlling for variation in developmental schedules across species in order to identify whether select developmental programs occur for an unusually long time in a given taxanomic group (Clancy et al. 2001; Charvet and Finlay 2018). To that end, we test whether a linear plateau captures *NEFH* expression over developmental time in the frontal cortex of both species. We then assess whether *NEFH* expression in the frontal cortex reaches a plateau significantly later in humans than in mice (Fig. 1*G*). *NEFH* expression in the frontal cortex increases with age to reach a plateau at 12 years of age in humans (easynls, model = 3, adjusted $R^2 = 0.954$, $P < 0.01$; $n = 7$); and reaches a plateau about 22 days after birth in mice (easynls, model = 3, age of plateau = PCD 40.5; adjusted $R^2 = 0.86$; $P < 0.01$; $n = 21$).

After controlling for variation in developmental schedules between the 2 species, *NEFH* expression reaches a plateau significantly later than expected in humans. That is, *NEFH* expression steadily increases until 12 years of age in humans. *NEFH* expression reaches a plateau at postconception day 40.5 (i.e., about 22 days after birth) in mice (Fig. 1*G*). According to the translating time model, a mouse on postconception day 38.5–42.5 (i.e., postnatal day 20–24) is approximately equivalent to a human at 1 year of age (postconception day 517; lower 95% CI: postconception day 399; upper 95% CI: postnatal day 671; Workman et al. 2013; http://translatingtime.org). If temporal changes in *NEFH* expression were conserved between humans and mice, *NEFH* expression should reach a plateau at approximately 1 year of age. Yet, the plateau in *NEFH* expression in the frontal cortex of humans is achieved at 12 years of age in humans, which is 11 years later than expected, and well above the confidence intervals generated from the translating time model. The increase in *NEFH* expression follow a protracted developmental time course in humans relative to the timing of most other developmental transformations (Fig. 1*G*). The protracted increase in *NEFH* expression is concomitant with increased frontal cortex *NEFH* expression in humans relative to mice (Fig. 1*G*). At its plateau, *NEFH* expression in the frontal cortex is 1.6 times greater in humans (Fig. 1*G*,*H*), and *NEFH* mRNA levels in the frontal cortex become significantly greater in humans ($x = 1.83$; SD = 0.13; $n = 3$) than in mice ($x = 0.14$; SD = 0.05; $n = 11$, $P < 0.05$; ks test; Fig. 1*H*). Thus, the protracted increase in *NEFH* expression is concomitant with an increase in *NEFH* expression in the adult human frontal cortex. These findings are consistent with the notion that there are major differences in cross-cortically connecting patterns between primates and mice, and these observations agree with those obtained from diffusion MR tractography, which together highlight major modifications to long-range cortically neurons between primates and mice. However, these data do not demonstrate whether the increase in *NEFH* expression observed in primates is due to an increase in *NEFH* expression in upper or lower layers.

We next assess whether there is variation in *NEFH* expression across cortical layers in humans and in mice. A relative increase in the expression of *NEFH* in upper layers of the cortex in primates suggests an increase in the number of corticocortical projecting neurons because corticocortical pathways preferentially emerge from layer II–III neurons. Importantly, however, some lower layer neurons do form corticocortical pathways. A previous report showed that the expression of *NEFH* appears increased in upper layers of the primary visual cortex of humans relative to mice (Zeng et al. 2012; Fig. 1*I*,*J*). To assess these differences quantitatively, we measured the area occupied by *NEFH* labeling in upper and lower layers in the primary visual cortex and the frontal cortex of humans and in mice. We then computed the density of *NEFH* expression in upper versus lower layers in both of these species in order to control for variation in background labeling across samples. A *t* test on the *NEFH* mRNA expression densities show that *NEFH* expression is relatively increased in upper versus lower layers in frontal cortical areas in humans ($x = 1.28$; SD = 0.17, $n = 6$) compared with mice ($x = 0.68$, SD = 0.23, $n = 6$, $t = 5.11$, $P < 0.05$, Fig. 1*K*). Similarly, *NEFH* expression is significantly more expressed in the primary visual cortex of humans ($x = 1.345$, SD = 0.40, $n = 5$) than in mice ($x = 0.72$, SD = 0.22, $n = 4$, $t = 3.04$, $P < 0.05$; Fig. 1*O*).

We identify species differences in developmental trajectories in *NEFH* expression in frontal cortical areas in humans and in mice, with a protracted increase in *NEFH* expression in upper layers in humans relative to mice after controlling for overall changes in developmental schedules (Supplementary Fig. S3). *NEFH* expression steadily increases up and subsequently plateaus at 20–28 years of age (equivalent to about 5 months of age in mice). In contrast, expression of *NEFH* in upper versus lower layers remains relatively stable throughout examined ages in mice. Taken together, these data highlight important heterochronic shifts in *NEFH* expression across layers between the 2 species.

To confirm that *NEFH* expression is indeed relatively reduced in upper layers in mice, we use a previously published single cell RNA sequencing dataset extracted from the primary visual cortex. The authors used the *t*-Distributed Stochastic Neighbor Embedding approach (tSNE) to identify subpopulations of cell types within the primary visual cortex. Such an approach identified excitatory neurons across different layers of the mouse visual cortex. We use this cell type assignment to test whether *NEFH* expression is indeed poorly expressed in excitatory in upper layer neurons. Consistent with our analyses comparing *NEFH* expression across upper and lower layers, the vast majority of *NEFH*-labeled excitatory neurons are indeed located in lower layers (i.e., layers V–VI) rather than in upper layers in mice (i.e., layers II–III; Fig. 1*L*,*O*). This situation holds for the primary visual cortex as well as the frontal cortex (Fig. 1*O*). These data suggest that primates may possess increased corticocortical pathways compared with mice.

Corticocortical Pathways in Relation to Cortical Folding

To investigate the evolution of corticocortical pathways among nonhuman primates, we place ROIs through similarly positioned cortical gyri in marmosets and in macaques (Figs 4 and 5). The placed ROIs across equivalent cortical regions (Fig. 4) identify a number of similarities but also some differences in connectivity patterns between the 2 species (Figs 4 and 5, Supplementary Fig. S7). Many of the highlighted fibers course across the anterior to posterior axis in macaques and marmosets, although some fibers course across the medial to lateral axes. Fibers coursing across the dorsal to ventral axes likely connect cortical and

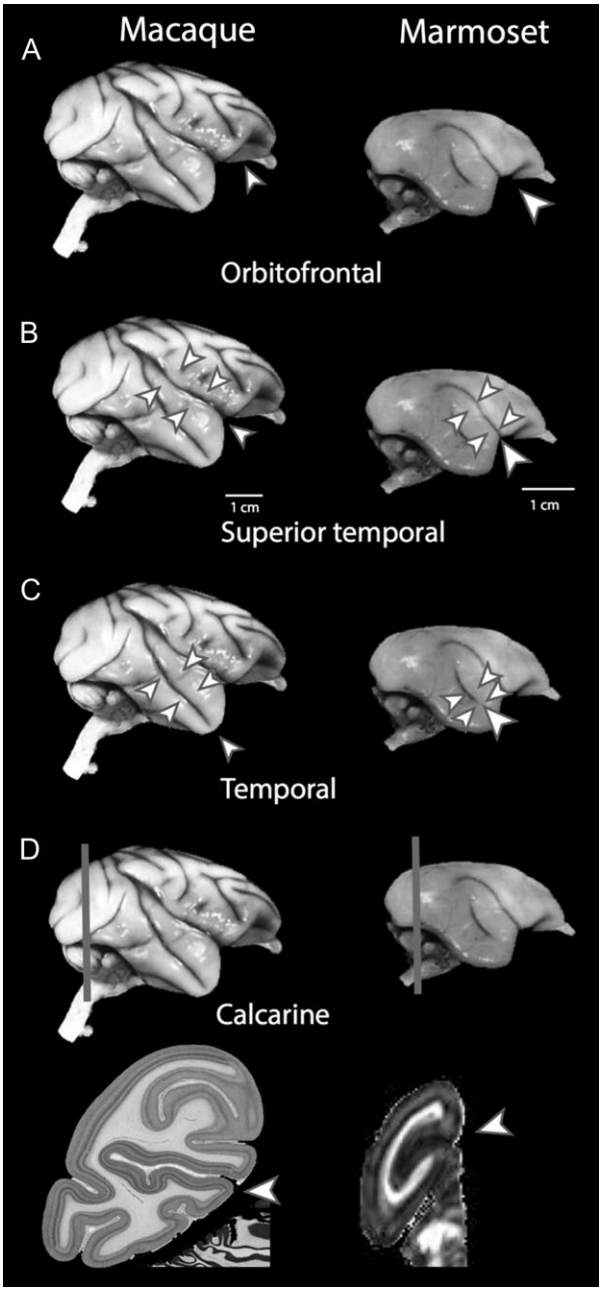

Figure 4. Arrowheads point to the location of ROIs placed through the macaque and marmoset cortex in order to identify corticocortical pathways coursing through these ROIs (Fig. 5). Arrowheads show the location of ROIs placed through the orbitofrontal (*A*), superior temporal (*B*) temporal (*C*) and calcarine sulci (*D*) of macaques and marmosets. (*D*) Vertical lines highlight approximate location through which coronal planes were taken. We use Nissl-stained sections through the macaque cortex and a coronal plane of a fractional anisotropy scan of the marmoset brain to highlight the location of ROIs through the calcarine sulcus.

subcortical structures whereas fibers coursing across the anterior to posterior or medial to lateral axes likely form corticocortical pathways (Charvet, Hof et al. 2017).

In both marmosets and macaques, ROIs placed in the orbitofrontal gyrus (Fig. 4A) show fibers coursing across the anterior to posterior axis between the frontal and temporal lobe, although the orbitofrontal gyrus in marmosets is shallow (Fig. 4A). Given that these fibers extend between the frontal and temporal lobes, we define these fibers as called the uncinate fasciculi. The uncinate fasciculus is observed in both macaques as in marmosets.

ROIs placed within the superior temporal gyrus (Fig. 4B) show that the fibers course tangentially to the main axes of sulci and gyri (see red arrows in Supplementary Fig. S7A and B). These fibers course medially and perpendicular to the sulci (see red arrows in Fig. 5B). Macaques and marmosets vary slightly in their overall trajectories. The macaque fibers course between ventral regions of the frontal lobe (Fig. 5B, yellow arrow) and the parietal lobe whereas similar fiber pathways in marmosets course between the ventral to dorsal regions of the frontal lobe.

ROIs placed within the temporal gyrus (Fig. 4C) highlight fibers in macaques and marmosets coursing across the anterior to posterior axis in the temporal lobe, which extend dorsally towards the occipital lobe (Fig. 5C). We define these fibers as the inferior longitudinal fasciculus (ILF) because these white matter fibers course across the anterior to posterior axis within the temporal lobe and connect with the occipital lobe. We note the presence of the ILF in marmosets and macaques (red arrows in Supplementary Fig. S7C and D). ILF fibers extend fine branches coursing medially and perpendicular to the sulcus (red arrows in Fig. 5C). ROIs placed within the calcarine sulcus show similar fiber trajectories in both macaques and marmosets; in addition to the optic radiation, pathways coursing from/to the temporal and frontal lobes are identified (Fig. 5D). Taken together, these data demonstrate that macaques and marmosets possess a number of corticocortical pathways.

Limbic and Cortico-subcortical Pathways

We clearly detect well-described pathways such as the cingulum, fornix, and thalamocortical and/or corticothalamic fibers (Fig. 5E–G). ROIs showed the cingulum, which courses across the anterior to posterior axis of the cortex across all 3 examined species. Marmoset and macaques possess branches coursing in 2 directions towards the frontal pole from the cingulum but the mouse cingulum fibers lack any type of branching extending across the anterior to posterior axis. Cingulum fibers in mice also appear thinner than in monkeys (see red circles in Fig. 5E). The macaque cingulum bundle spans its horizontal axis, while the marmoset cingulum bundle appears to be angled slightly upwards in its trajectory (see blue arrows in Fig. 5E). At the posterior end of the bundle, the macaque cingulum remains flat, while the marmoset bundle curves downward. In mice, the fornix lacked curvature in comparison to that of the monkey (see red arrows in Fig. 5F). The macaque and marmoset thalamocortical/corticothalamic fibers begin and terminate at similar corresponding locations (see red and yellow circles in Fig. 5G). In mice, fibers protrude towards the superior region of the frontal lobe (see black circles in Fig. 5G). In the primate brains, the fibers protrude in different directions from the origin point and span more cortical territory (see blue arrows in Fig. 5G). Thus, diffusion MR tractography successfully traces these pathways despite variation in brain geometry and size across the examined species.

We confirm our tractography results with those obtained from tract-tracers, made available by the Allen Brain Atlas (Supplementary Fig. S1; Oh et al. 2014). The injection site in the Allen Brain Atlas ROIs from diffusion MR tractographies in the corresponding regions identify the cingulum bundle (Supplementary Fig. S1A, red arrows), a part of the fornix (Supplementary Fig. S1B, red arrows), a part of the thalamocortical pathways (Supplementary Fig. S1C, red arrows), and a part of the corpus callosal pathways

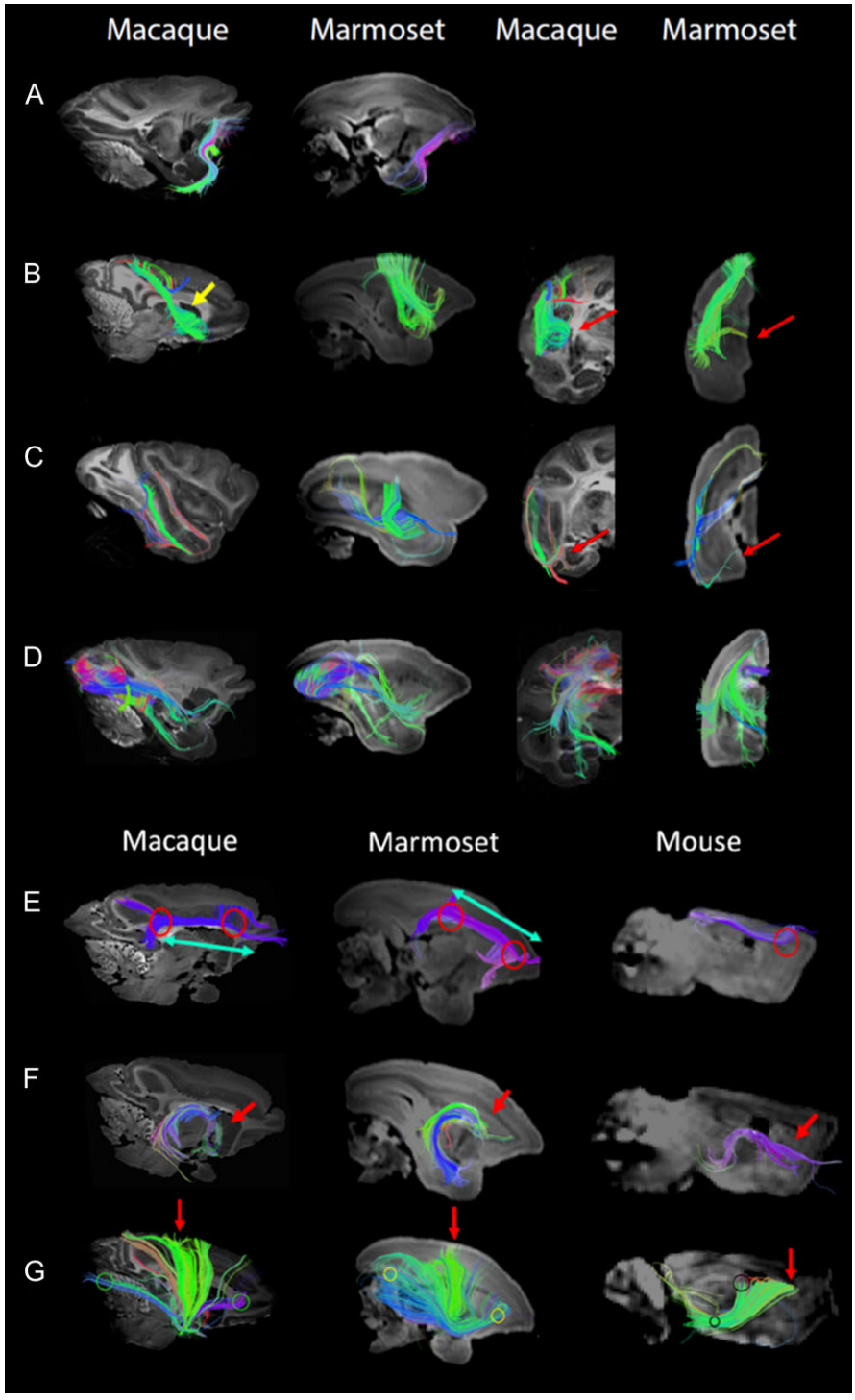

Figure 5. Panels (*A–D*) show fibers coursing through ROIs as shown in Figure 4. (*A*) ROIs show fibers coursing through the inferior orbitofrontal gyrus in macaques and marmosets. We define these fibers as the uncinate fasciculus given that they course between the frontal and temporal lobe. We note that the uncinate fasciculus is present in both macaques and marmosets and that these fibers principally course across the anterior to posterior axis. (*B*) Sagittal and coronal slices of fibers course through the superior temporal areas. These fibers course across the medial to lateral axis and are observed in both macaques and marmosets. (*C*) Coronal and sagittal slices of fibers course through the temporal areas. In both macaques and marmosets, fibers course across the anterior to posterior axis between the frontal and temporal lobes. They satisfy our definition of the ILF. (*D*) Sagittal and coronal slices through the calcarine sulcus highlight fibers coursing across the anterior to posterior axis. We successfully traced the cingulum bundle (*E*), fornix (*F*), and thalamocortical or corticothalamic (*G*) fibers in macaques, marmosets, and mice.

(Supplementary Fig. S1*D*, red arrows). Lateral long-range pathways detected from diffusion MR tractography are concordant with those obtained from tract-tracers (Supplementary Fig. S1*A*, *B*, yellow arrows).

Discussion

In this study, we consider the 3D perspective offered from high-resolution diffusion MR tractography to investigate the

evolution of cortical pathways across euarchontoglires. Despite some species differences in branching patterns and variation in the number of cortical pathways coursing in different directions in macaques versus marmosets, our results highlight many similarities in patterns of connectivity between the 2 species (Zhang et al. 2013). At least some of these fibers we describe emerged early in primate evolution with or possibly before the emergence of haplorrhine primates (i.e., monkeys, apes). Our comparative analyses of *NEFH* expression coupled with white matter scaling, and diffusion MR tractography demonstrates that primates deviate from mice in possessing alterations in corticocortical pathways.

Methodological Approaches

The rapid acquisition of information from noninvasive scans coupled with the 3D perspective offered from diffusion MR tractography provides a high-throughput approach with which to study the evolution and development of connections across species (Schwartz et al. 1991; Takahashi et al. 2010, 2012; Li et al. 2014; Song et al. 2015). Diffusion MR imaging, as with any other method, does have some limitations. For instance, diffusion MR tractography has difficulty resolving the precise terminations of pathways within the gray matter (Jones et al. 2013), which is especially challenging when comparing brains differing in size and structure. Diffusion MR tractography may also preferentially identify pathways based on certain characteristics (axon length, myelination) and neglect to identify other fibers (Reveley et al. 2015; Schilling et al. 2018). How best to resolve crossing fibers is an ongoing venue for research (Wedeen et al. 2008; Maier-Hein et al. 2017; Schilling, Gao, Stepniewska et al. 2017). Diffusion spectrum and high angular resolution diffusion imaging can theoretically resolve crossing fibers (Takahashi et al. 2010, 2011, 2012), as well as pathways in poorly myelinated regions (Wilkinson et al. 2017). Indeed, our diffusion MR tractography successfully traced a number of well-characterized pathways. That is, we identified the fornix, cingulum bundle, thalamocortical or corticothalamic pathways with diffusion MRI tractography, which validates its use for cross-species comparisons. However, due to the potential limitations of diffusion MR tractography, we do not focus on detecting the precise terminations of pathways within the gray matter. Rather, we identify pathways coursing through similarly positioned cortical gyri and sulci. It is also for these reasons that we adopt a descriptive rather than a quantitative approach, and we integrate observations from diffusion MR tractography with comparative analyses of *NEFH* expression, and white matter scaling between primates and rodents.

Our tractography study is descriptive and some quantification might help to improve the work. However, we only have 2 samples in each species, in which case quantification will not be reliable and may introduce another type of uncertainty. Measures from 2 samples in each species may not be enough to quantitatively conclude measures across species. Therefore, we qualitatively reported tractography results in this study.

While the diffusion MRI technique has many positive attributes, it is not without limitations. Irrespective of the use of different algorithms, researchers are aware that standard approaches of diffusion MR tractography suffer from their limitations (Thomas et al. 2014; Chen et al. 2015; Neto Henriques et al. 2015; Takemura et al. 2016). It is possible that one can find extremely variable results using the same diffusion MRI data, which could be instructive as a clear warning to researchers interested in MR tractography methods, and various tractography settings need to be used when tracking through subcortical brain regions, depending on the type of pathways. Since the brain structure is complex and axonal fibers take elaborate routes, it is likely that we need to define optimal sets of tractography parameters, not only at the gray/white matter border but also in many other brain regions such as the subcortical nuclei (thalamus, hippocampus, deep cerebellar nuclei, etc.) and specific brain regions where we know fibers are extensively crossing. It is therefore important to find optimal fiber reconstruction settings in each brain region, as well as optimal combinations of such parameters across brain regions, in order to significantly increase imaging accuracy of whole brain fiber pathways. This problem exists in tractography of any species.

Evolution of Long-Range Corticocortical Pathways

The results from the present study quantitatively confirm that *NEFH* expression, a marker that identifies neurons projecting over long distances, is more strongly expressed in select cortical areas of primates compared with mice. We assessed whether the increase in *NEFH* expression in the primate cortex may result, at least in part, from an increase in *NEFH* expression in upper layers because layer II–III neurons preferentially form corticocortical pathways. Indeed, *NEFH* is significantly more expressed in upper layers of the cortex in humans than in mice. Our findings are in agreement with those of Zeng et al. 2012 who reported that *NEFH* is preferentially expressed in upper layers of the primary visual cortex in humans compared with mice. However, the study by Zeng et al. 2012 does not distinguish whether *NEFH* expression is increased in humans or whether the *NEFH* expression is shifted from lower to upper layers in humans. Although we did not test for differences in *NEFH* mRNA expression across the entire isocortex of humans versus mice, the present study demonstrates that *NEFH* mRNA expression is significantly increased in the frontal cortex and the primary visual cortex of humans. The increase in *NEFH* expression is concomitant with a relative increase in upper layer neurons in humans. These findings are consistent with the notion that humans possess increased corticocortical pathways compared with mice. Observations from diffusion MR data tractography highlight that the primate cortex contains a number of corticocortical pathways coursing in various directions through the white matter of the cortex. This is in contrast with mice where only a relatively few cortical pathways (e.g., corpus callosum, cingulum) are observed coursing across white matter of the isocortex (Fig. 1). For a given brain size, the cortical white matter volume is disproportionately enlarged in primates versus rodents (Fig. 3). Thus, the data from diffusion MR tractography, white matter scaling, and *NEFH* mRNA expression converge to show that primates possess increased corticocortical projecting neurons compared with mice.

The present study showed that cortical *NEFH* expression patterns are protracted in humans relative to mice (Figs 1 and 2; Supplementary Fig. S3). After controlling for species differences in developmental schedules, we found that it takes longer for humans to reach adult levels of *NEFH* expression in the frontal cortex than it does for mice. These findings suggest that all or a subset of neural pathways originating from the cortex are protracted in humans compared with other species. It would, therefore, be of interest to identify whether heterochronic shifts in *NEFH* expression associate with protracted growth of brain pathways, and whether such delays are concomitant with protracted behavioral development across humans, nonhuman primates, and rodents.

Evolution of Long-Range Corticocortical Pathways in Primates

We set ROIs through the cortex of primates to identify long-range cortical pathways. The vast majority of these ROIs identified pathways forming corticocortical pathways rather than pathways connecting cortical and subcortical structures. We also observed that the cortical white matter is disproportionately expanded in primates compared with rodents. These data are consistent with the notion that primates possess a large number of corticocortical pathways (Figs 3 and 5). We observed fibers coursing across the anterior to posterior direction of the cortex in macaques as in marmosets. Those include the ILF and the uncinate fasciculus. The ILF may consist of a series of fibers coursing across the anterior to posterior axes of the cortex and/or a series of long association fibers coursing between the occipital and temporal lobes (Tusa and Ungerleider 1985; Catani et al. 2003; Schmahmann et al. 2007). We also observe fibers coursing from the frontal to temporal lobes, which we define as the uncinate fasciculus. We here do not use diffusion MR tractography to detect the precise start or end location of these fibers. Previous tract-tracer studies and diffusion MR tractography studies noted that the ILF and uncinate fasciculus are present in humans and macaques but that it is either small or nonexistent in rodents, or carnivores (Schmahmann et al. 2007; Schmahmann and Pandya 2009; Takahashi et al. 2010a,b; Charvet, Hof et al. 2017). The finding that the ILF and uncinate fasciculi are present in marmosets suggests that the ILF and uncinate fasciculus evolved relatively early in primate evolution, with or before the emergence of haplorhine primates (i.e., monkeys, apes). It would be of interest to investigate whether the ILF and uncinate fasciculus are present in strepsirhine primates (e.g., lemurs) to trace the emergence of the ILF and uncinate fasciculus within the euarchontoglire lineage.

Developmental Source of Variation in Connectivity Patterns

The observed differences in corticocortical pathways between primates and rodents can be traced back to developmental differences that serve to generate variation in the cortical composition between primates and rodents. Cortical neurogenesis occurs for an unusually long time in primates compared with rodents, even after controlling for overall variation in developmental schedules (Clancy et al. 2001; Charvet, Šimić et al. 2017). The consequence of extending the duration of cortical neurogenesis during development is that primates possess disproportionately more cortical neurons in adulthood. Most of the increase in cortical neuron numbers is accounted for by upper layer neurons (layers II–IV; Charvet et al. 2015; Srinivasan et al. 2015; Charvet, Hof et al. 2017; Charvet, Šimić et al. 2017; Charvet, Stimpson et al. 2017; Atapour et al. 2018). Cortical neurogenesis onset is roughly similar between primates and rodents, but cortical neurogenesis is extended for longer than expected considering the timing of most other developmental transformations. As a result, layer IV and layer II–III neurons are produced for much longer than expected in primates than in rodents (Clancy et al. 2001; Charvet et al. 2011; Workman et al. 2013; Charvet, Šimić et al. 2017). Accordingly, extending the duration of cortical neurogenesis should lead to a concomitant amplification of local circuit layer IV neurons as well as layer II–III neurons forming long-range corticocortical pathways (Cahalane et al. 2014).

The expansion of upper layer neuron numbers in primates might be due to both increased local circuit layer IV neurons and increased long-range corticocortical pathways originating from layers II–III. In support of this finding is the observation that *NEFH*-labeled neuron numbers appear to increase progressively with laminar differentiation. Areas with highly differentiated cytoarchitectural variation (i.e., layer IV) give rise to increased layer II–III long-range corticocortical pathways (Barbas and García-Cabezas 2016; Barbas et al. 2018). However, the relative contribution of layer III versus layer IV have yet to be quantified systematically across primates and rodent species.

Many of corticocortical pathways described in primates (e.g., ILF, superior longitudinal fasciculus, uncinate fasciculus, arcuate fasciculus; Schmahmann et al. 2007; Schmahmann and Pandya 2009) course across the anterior to posterior axes. Many of these pathways are not readily observed in other mammalian species (Takahashi et al. 2010; Charvet, Hof et al. 2017). Primates may deviate from other mammals in possessing increased anterior to posterior corticocortical integration. The direction of these pathways align, at least to some extent, with variation in upper layer neuron numbers under a unit of cortical surface area, with upper layer neuron numbers varying from high values in the posterior cortex to low neuron numbers per unit of cortical surface area towards the frontal cortex (Charvet et al. 2015). Thus, long-range anterior to posterior corticocortical integration observed in primates aligns with the spatial variation in neuronal numbers under the cortical surface.

Corticocortical Projections and Gyrification

A number of studies and hypotheses have considered how developmental processes may generate evolutionary changes in cortical composition, as well as gyrification across species (Goldman-Rakic et al. 1984; Sun and Hevner 2014; Striedter et al. 2015). An influential hypothesis posits that tension generated by short-range axons pull interconnected cortical regions together and cause gyrification (Van Essen 1997), although a number of other explanations have been offered. The differential growth across the cortex, the migration of neurons along radial glia, and/or the differential expansion of upper versus lower layer neurons are a few proposed mechanisms generating variation in cortical folding between species (Richman et al. 1975; Van Essen 1997; Toro and Burnod 2005; Xu et al. 2010; Chen et al. 2013; Striedter et al. 2015; Fernández et al. 2016; Tallinen et al. 2016; Razavi et al. 2017). Modifications to neurogenetic programs are well-documented sources of variation across species, and experimental manipulations of cell proliferation during development impact cortical composition, as well as cortical folding (Dyer et al. 2009; Clowry et al. 2010; Charvet and Striedter 2008, 2011; Lewitus et al. 2013; McGowan et al. 2012, 2013; Nonaka-Kinoshita et al. 2013; Borrell and Götz 2014; Otani et al. 2016; Tallinen et al. 2016; Toda et al. 2016; Charvet, Hof et al. 2017; Charvet, Šimić et al. 2017; de Juan Romero and Borrell 2017; Matsumoto et al. 2017; Shinmyo et al. 2017). We suggest that the differential composition of neurons across the depth of the cortex may cause major differences in white matter tension between species. Variation in cortical tension may, in turn, differentially impact cortical folding between mammalian orders (Pillay and Manger 2007; Zilles et al. 2013). Modifications to cortical composition and projection patterns evolve in concert, and may together lead to major differences in the extent of cortical folding between primates and rodents. Although the precise mechanisms generating buckling of the cortex is an ongoing matter of debate, it is likely that a number of coordinated factors, rather than a single factor, dictate the extent and spatial variation of cortical folds.

Supplementary Material

Supplementary material is available at *Cerebral Cortex* online.

Funding

This work was funded by the Eunice Shriver Kennedy National Institute of Child Health and Development (NICHD) (R01HD078561, R21HD069001) (E.T.), the National Institute of Mental Health (R21MH118739) (E.T.), the National Institute of Neurological Disorders and Stroke (R03NS091587) (E.T.), as well as grant number P20GM103653 from the National Institute of General Medicine Sciences for research at Delaware State University. This research was carried out in part at the Athinoula A. Martinos Center for Biomedical Imaging at the Massachusetts General Hospital, using resources provided by the Center for Functional Neuroimaging Technologies, NIH P41RR14075, a P41 Regional Resource supported by the Biomedical Technology Program of the National Center for Research Resources (NCRR), National Institutes of Health. This work also involved the use of instrumentation supported by the NCRR Shared Instrumentation Grant Program (S10RR023401, S10RR019307, and S10RR023043), and High-End Instrumentation Grant Program (S10RR016811).

Notes

We thank Drs. Guangping Dai and Lana Vasung for providing technical assistance, and Dr. Marnin Wolfe for statistical advice. Some MRI scans used in the analyses are made available thanks to Dr Roberto Toro via the www.braincatalog.org. We thank Drs Muñoz-Moreno, Radtke-Schuller, and Eike Budinger for extended access to the rabbit and gerbil MR atlases. We thank Dr Shintaku for access to the pygmy marmoset brain scan via the Japan Monkey Centre Primates Brain Imaging Repository for comparative neuroscience. Photos of mouse, macaque, and marmoset brains are from the comparative mammalian brain collection (http://neurosciencelibrary.org). Images of tract-tracer studies, *NEFH* in situ hybridization data from mice and humans were taken from the Allen Institute Website and the Brainspan atlas of the developing human brain. These data are available at http://developingmouse.brain-map.org and at http://www.brainspan.org, which are supported by the National Institute of Health Contract HHSN-271-2008-00 047-C to the Allen Institute for Brain Science. The opinions in this article are not necessarily those of the NIH. *Conflict of Interest*: None declared.

References

Atapour N, Majka P, Wolkowicz IH, Malamanova D, Worthy KH, Rosa MG. 2018. Neuronal distribution across the cerebral cortex of the marmoset monkey (*Callithrix jacchus*). Cereb Cortex. In Press.

Barbas H. 1986. Pattern in the laminar origin of corticocortical connections. J Comp Neurol. 252:415–422.

Barbas H. 2015. General cortical and special prefrontal connections: principles from structure to function. Annu Rev Neurosci. 38:269–289.

Barbas H, García-Cabezas MÁ. 2016. How the prefrontal executive got its stripes. Curr Opin Neurobiol. 40:125–134.

Barbas H, Hilgetag CC, Saha S, Dermon CR, Suski JL. 2005. Parallel organization of contralateral and ipsilateral prefrontal cortical projections in the rhesus monkey. BMC Neurosci. 6:32.

Barbas H, Medalla M, Alade O, Suski J, Zikopoulos B, Lera P. 2005. Relationship of prefrontal connections to inhibitory systems in superior temporal areas in the rhesus monkey. Cereb Cortex. 15:1356–1370.

Barbas H, Rempel-Clower N. 1997. Cortical structure predicts the pattern of corticocortical connections. Cereb Cortex. 7: 635–646.

Barbas H, Wang J, Joyce MKP, Garcia-Cabezas MA. 2018. Pathway mechanism for excitatory and inhibitory control in working memory. J Neurophysiol. 120:2659–2678.

Beul SF, Barbas H, Hilgetag CC. 2017. A predictive structural model of the primate connectome. Sci Rep. 7:43176.

Bininda-Emonds OR, Cardillo M, Jones KE, MacPhee RD, Beck RM, Grenyer R, Price SA, Vos RA, Gittleman JL, Purvis A. 2007. The delayed rise of present-day mammals. Nature. 446:507–512.

Bons N, Sihol S, Barbier V, Mestre-Frances N, Albe-Fessard D. 1998. A stereotaxic atlas of the grey lesser mouse lemur brain (Microcebus murinus). Amsterdam: Elsevier.

Borrell V, Götz M. 2014. Role of radial glial cells in cerebral cortex folding. Curr Opin Neurobiol. 27:39–46.

Bozek K, Wei Y, Yan Z, Liu X, Xiong J, Sugimoto M, Tomita M, Pääbo S, Pieszek R, Sherwood CC, et al. 2014. Exceptional evolutionary divergence of human muscle and brain metabolomes parallels human cognitive and physical uniqueness. PLoS Biol. 12:e1001871.

Cahalane DJ, Charvet CJ, Finlay BL. 2014. Modeling local and cross-species neuron number variations in the cerebral cortex as arising from a common mechanism. Proc Natl Acad Sci USA. 111:17642–17647.

Campbell MJ, Morrison JH. 1989. Monoclonal antibody to neurofilament protein (SMI-32) labels a subpopulation of pyramidal neurons in the human and monkey neocortex. J Comp Neurol. 282:191–205.

Catani M, de Schotten MT. 2008. A diffusion tensor imaging tractography atlas for virtual in vivo dissections. Cortex. 44: 1105–1132.

Catani M, Jones DK, Donato R, Ffytche DH. 2003. Occipito-temporal connections in the human brain. Brain. 126:2093–2107.

Charvet CJ, Cahalane DJ, Finlay BL. 2015. Systematic, cross-cortex variation in neuron numbers in rodents and primates. Cereb Cortex. 25:147–160.

Charvet CJ, Finlay BL. 2018. Comparing adult hippocampal neurogenesis across species: translating time to predict the tempo in humans. Front Neurosci. 12:706.

Charvet CJ, Hof PR, Raghanti MA, Kouwe AJ, Sherwood CC, Takahashi E. 2017. Combining diffusion magnetic resonance tractography with stereology highlights increased cross-cortical integration in primates. J Comp Neurol. 525:1075–1093.

Charvet CJ, Stimpson CD, Kim YD, Raghanti MA, Lewandowski AH, Hof PR, Gómez-Robles A, Krienen FM, Sherwood CC. 2017. Gradients in cytoarchitectural landscapes of the isocortex: diprotodont marsupials in comparison to eutherian mammals. J Comp Neurol. 525:1811–1826.

Charvet CJ, Striedter GF. 2008. Developmental species differences in brain cell cycle rates between northern bobwhite quail (*Colinus virginianus*) and parakeets (*Melopsittacus undulatus*): implications for mosaic brain evolution. Brain Behav Evol. 72:295–306.

Charvet CJ, Striedter GF. 2011. Developmental modes and developmental mechanisms can channel brain evolution. Front Neuroanat. 5:4.

Charvet CJ, Striedter GF, Finlay BL. 2011. Evo-devo and brain scaling: candidate developmental mechanisms for variation and constancy in vertebrate brain evolution. Brain Behav Evol. 78:248–257.

Charvet CJ, Šimić G, Kostović I, Knezović V, Vukšić M, Leko MB, Takahashi E, Sherwood CC, Wolfe MD, Finlay BL. 2017. Coevolution in the timing of GABAergic and pyramidal neuron maturation in primates. Proc R Soc B. 284. pii: 20171169.

Chen H, Liu T, Zhao Y, Zhang T, Li Y, Li M, Zhang H, Kuang H, Guo L, Tsien JZ, et al. 2015. Optimization of large-scale mouse brain connectome via joint evaluation of DTI and neuron tracing data. Neuroimage. 115:202–213.

Chen H, Zhang T, Guo L, Li K, Yu X, Li L, Yu X, Li L, Hu X, Han J, et al. 2013. Coevolution of gyral folding and structural connection patterns in primate brains. Cereb Cortex. 23: 1208–1217.

Clancy B, Darlington RB, Finlay BL. 2001. Translating developmental time across mammalian species. Neurosci. 105:7–17. doi.org/10.1016/S0306-4522(01)00171-3.

Clowry G, Molnár Z, Rakic P. 2010. Renewed focus on the developing human neocortex. J Anat. 217:276–288.

Cohen AH, Wang R, Wilkinson M, MacDonald P, Lim AR, Takahashi E. 2016. Development of human white matter fiber pathways: From newborn to adult ages. Int J Dev Neurosci. 50:26–38.

Das A, Takahashi E. 2017. Characterization of white matter tracts by diffusion tractography in cat and ferret that have similar gyral patterns. Cereb Cortex. 10:1–10.

de Juan Romero C, Borrell V. 2017. Genetic maps and patterns of cerebral cortex folding. Curr Opin Cell Biol. 49:31–37.

Dyer MA, Martins R, da Silva Filho M, Muniz JA, Silveira LCL, Cepko C, Finlay BL. 2009. Developmental sources of conservation and variation in the evolution of the primate eye. Proc Natl Acad Sci USA. 106:8963–8968.

Edlow BL, Takahashi E, Wu O, Benner T, Dai G, Bu L, Grant PE, Greer DM, Greenberg SM, Kinney HC, et al. 2012. Neuroanatomic connectivity of the human ascending arousal system critical to consciousness and its disorders. J Neuropathol Exp Neurol. 71:531–546.

Fame R, MacDonald J, Dunwoodie S, Takahashi E, Macklis J. 2016. Cited2 regulates neocortical layer II/III generation and somatosensory callosal projection neuron development and connectivity. J Neurosci. 36:6403–6419.

Fernández V, Llinares-Benadero C, Borrell V. 2016. Cerebral cortex expansion and folding: what have we learned? EMBO J. 35:e201593701.

Freckleton RP, Harvey PH, Pagel M. 2000. Phylogenetic analysis and comparative data: a test and review of evidence. Am Nat. 160:712–726.

Friedland DR, Popper P, Eernisse R, Ringger B, Cioffi JA. 2006. Differential expression of cytoskeletal genes in the cochlear nucleus. Anat Rec A Discov Mol Cell Evol Biol. 288:447–465.

Gilbert CD, Kelly JP. 1975. The projections of cells in different layers of the cat's visual cortex. J Comp Neurol. 163:81–105.

Goldman-Rakic PS, Rakic P. Geschwind N, Galaburda A. 1984. Experimental modification of gyral patterns. In: Cerebral dominance: biological foundations. Cambridge, MA: Harvard University Press. p. 179–192.

Goulas A, Zilles K, Hilgetag CC. 2018. Cortical gradients and laminar projections in mammals. Trends in Neurosci. 41: 775–788.

Hilgetag CC, Grant S. 2010. Cytoarchitectural differences are a key determinant of laminar projection origins in the visual cortex. Neuroimage. 51:1006–1017.

Hilgetag CC, Medalla M, Beul SF, Barbas H. 2016. The primate connectome in context: principles of connections of the cortical visual system. Neuroimage. 134:685–702.

Hof PR, Nimchinsky EA, Morrison JH. 1995. Neurochemical phenotype of corticocortical connections in the macaque monkey: Quantitative analysis of a subset of neurofilament protein-immunoreactive projection neurons in frontal, parietal, temporal, and cingulate cortices. J Comp Neurol. 362: 109–133.

Hofman MA. 2014. Evolution of the human brain: when bigger is better. Front Neuronat. 8:15.

Horvát S, Gămănuț R, Ercsey-Ravasz M, Magrou L, Gămănuț B, Van Essen DC, Burkhalter A, Knoblauch K, Toroczkai Z, Kennedy H. 2016. Spatial embedding and wiring cost constrain the functional layout of the cortical network of rodents and primates. PLoS Biol. 14:e1002512.

Hrvatin S, Hochbaum DR, Nagy MA, Cicconet M, Robertson K, Cheadle L, Zilionis R, Ratner A, Borges-Monroy R, Klein AM, et al. 2018. Single-cell analysis of experience-dependent transcriptomic states in the mouse visual cortex. Nat Neurosci. 21:120–129.

Jones DK, Knösche TR, Turner R. 2013. White matter integrity, fiber count, and other fallacies: the dos and don'ts of diffusion MRI. Neuroimage. 73:239–254.

Kaas JH. 2012. The evolution of neocortex in primates. Prog Brain Res. 195:91–102.

Kanamaru Y, Li J, Stewart N, Sidman RL, Takahashi E. 2017. Cerebellar pathways in mouse model of Purkinje cell degeneration detected by high-angular resolution diffusion imaging tractography. Cerebellum. 16:648–655.

Kennedy H, Bullier J. 1985. A double-labeling investigation of the afferent connectivity to cortical areas V1 and V2 of the macaque monkey. J Neurosci. 10:2815–2830.

Kolasinski J, Takahashi E, Stevens AA, Benner T, Fischl B, Zöllei L, Grant PE. 2013. Radial and tangential neuronal migration pathways in the human fetal brain: anatomically distinct patterns of diffusion MRI coherence. Neuroimage. 79:412–422.

Lewitus E, Kelava I, Huttner WB. 2013. Conical expansion of the outer subventricular zone and the role of neocortical folding in evolution and development. Front Human Neurosci. 7:424.

Li G, Wang L, Shi F, Lyall AE, Lin W, Gilmore JH, Shen D. 2014. Mapping longitudinal development of local cortical gyrification in infants from birth to 2 years of age. J Neurosci. 34: 4228–4238.

Lister R, Mukamel EA, Nery JR, Urich M, Puddifoot CA, Johnson ND, Lucero J, Huang Y, Dwork AJ, Schultz MD, et al. 2013. Global epigenomic reconfiguration during mammalian brain development. Science. 341:1237905. PMID: 23828890.

Maier-Hein KH, Neher PF, Houde JC, Côté MA, Garyfallidis E, Zhong J, Chamberland M, Yeh FC, Lin YC, Ji Q, et al. 2017. The challenge of mapping the human connectome based on diffusion tractography. Nat Commun. 8:1349.

Manocha SL. 1979. Physical growth and brain development of captive-bred male and female squirrel monkeys, Saimiri sciureus. Experientia. 35:96–98.

Marszalek JR, Williamson TL, Lee MK, Xu Z, Hoffman PN, Becher MW, Crawford TO, Cleveland DW. 1996. Neurofilament subunit NF-H modulates axonal diameter by selectively slowing neurofilament transport. J Cell Biol. 135: 711–724.

Matsumoto N, Shinmyo Y, Ichikawa Y, Kawasaki H. 2017. Gyrification of the cerebral cortex requires FGF signaling in the mammalian brain. Elife. 6:e29285.

McGowan LD, Alaama RA, Freise AC, Huang JC, Charvet CJ, Striedter GF. 2012. Expansion, folding, and abnormal lamination of the chick optic tectum after intraventricular

injections of FGF2. Proc Natl Acad Sci USA. 109(Supplement 1):10640–10646.
McGowan LD, Alaama RA, Striedter GF. 2013. FGF2 delays tectal neurogenesis, increases tectal cell numbers, and alters tectal lamination in embryonic chicks. PLoS One. 8:e79949.
McNab JA, Jbabdi S, Deoni SC, Douaud G, Behrens TE, Miller KL. 2009. High resolution diffusion-weightedimaging in fixed human brain using diffusion-weighted steady state free precession. Neuroimage. 46:775–785.
Mortazavi F, Oblak AL, Morrison WZ, Schmahmann JD, Stanley HE, Wedeen VJ, Rosene DL. 2017. Geometric navigation of axons in a cerebral pathway: comparing dMRI with tract tracing and immunohistochemistry. Cereb Cortex. 28:1–14.
Muñoz-Moreno E, Arbat-Plana A, Batalle D, Soria G, Illa M, Prats-Galino A, Eixarch E, Gratacos E. 2013. A magnetic resonance image based atlas of the rabbit brain for automatic parcellation. PLoS One. 8:e67418.
Nadkarni NA, Bougacha S, Garin C, Dhenain M, Picq JL. 2018. Digital templates and brain atlas dataset for the mouse lemur primate. Data Brief. 21:1178–1185.
Neto Henriques R, Correia MM, Nunes RG, Ferreira HA. 2015. Exploring the 3D geometry of the diffusion kurtosis tensor–impact on the development of robust tractography procedures and novel biomarkers. Neuroimage. 111:85–99.
Nguyen MQ, Wu Y, Bonilla LS, von Buchholtz LJ, Ryba NJ. 2017. Diversity amongst trigeminal neurons revealed by high throughput single cell sequencing. PLoS One. 12:e0185543.
Nonaka-Kinoshita M, Reillo I, Artegiani B, Martínez-Martínez MÁ, Nelson M, Borrell V, Calegari F. 2013. Regulation of cerebral cortex size and folding by expansion of basal progenitors. EMBO J. 32:1817–1828.
Nudo RJ, Masterton RB. 1988. Descending pathways to the spinal cord: a comparative study of 22 mammals. J Comp Neurol. 277:53–79.
Nudo RJ, Masterton RB. 1990. Descending pathways to the spinal cord, III: sites of origin of the corticospinaltract. J Comp Neurol. 296:559–583.
Okano H, Mitra P. 2015. Brain-mapping projects using the common marmoset. Neuroscience Res. 93:3–7.
Oh SW, Harris JA, Ng L, Winslow B, Cain N, Mihalas S, Wang Q, Lau C, Kuan L, Henry AM, et al. 2014. A mesoscale connectome of the mouse brain. Nature. 508:207.
Otani T, Marchetto MC, Gage FH, Simons BD, Livesey FJ. 2016. 2D and 3D stem cell models of primate cortical development identify species-specific differences in progenitor behavior contributing to brain size. Cell Stem Cell. 18:467–480.
Pagel M. 1999. Inferring the historical patterns of biological evolution. Nature. 401:877–884.
Pandya DN, Kuypers HG. 1969. Cortico-cortical connections in the rhesus monkey. Brain Res. 13:13–36.
Perelman P, Johnson WE, Roos C, Seuánez HN, Horvath JE, Moreira MA, Kessing B, Pontius J, Roelke M, Rumpler Y, et al. 2011. A molecular phylogeny of living primates. PLoS Genet. 7:e1001342.
Pillay P, Manger PR. 2007. Order-specific quantitative patterns of cortical gyrification. Eur J Neurosci. 25:2705–2712.
Radtke-Schuller S, Schuller G, Angenstein F, Grosser OS, Goldschmidt J, Budinger E. 2016. Brain atlas of the Mongolian gerbil (*Meriones unguiculatus*) in CT/MRI-aided stereotaxic coordinates. Brain Struct Funct. 221:1–272.
Razavi MJ, Zhang T, Chen H, Li Y, Platt S, Zhao Y, Guo L, Hu X, Wang X, Liu T. 2017. Radial structure scaffolds convolution patterns of developing cerebral cortex. Front Comput Neurosci. 11:76.
Reveley C, Seth AK, Pierpaoli C, Silva AC, Yu D, Saunders RC, Frank QY. 2015. Superficial white matter fiber systems impede detection of long-range cortical connections in diffusion MR tractography. Proc Natl Acad Sci USA. 112: E2820–E2828.
Richman DP, Stewart RM, Hutchinson JW, Caviness VS Jr. 1975. Mechanical model of brain convolutional development. Science. 189:18–21.
Rilling JK. 2014. Comparative primate neuroimaging: insights into human brain evolution. Trends Cogn Sci. 18:46–55.
Rilling JK, Glasser MF, Preuss TM, Ma X, Zhao T, Hu X, Behrens TE. 2008. The evolution of the arcuate fasciculus revealed with comparative DTI. Nat Neurosci. 11:426.
Sakai T, Hata J, Ohta H, Shintaku Y, Kimura N, Ogawa Y, Sogabe K, Mori S, Okano HJ, Hamada Y, et al. 2018. The Japan Monkey Centre Primates Brain Imaging Repository for comparative neuroscience: an archive of digital records including records for endangered species. Primates. 59: 553–570.
Saunders A, Macosko EZ, Wysoker A, Goldman M, Krienen FM, de Rivera H, Bien E, Baum M, Bortolin L, Wang S, et al. 2018. Molecular diversity and specializations among the cells of the adult mouse brain. Cell. 174:1015–1030.
Schilling K, Gao Y, Janve V, Stepniewska I, Landman BA, Anderson AW. 2017. Can increased spatial resolution solve the crossing fiber problem for diffusion MRI? NMR Biomed. 30:e3787.
Schilling K, Gao Y, Janve V, Stepniewska I, Landman BA, Anderson AW. 2018. Confirmation of a gyral bias in diffusion MRI fiber tractography. Hum Brain Mapp. 39:1449–1466.
Schilling KG, Gao Y, Stepniewska I, Wu TL, Wang F, Landman BA, Gore JC, Chen LM, Anderson AW. 2017. The VALiDATe29 MRI based multi-channel atlas of the squirrel monkey brain. Neuroinformatics. 15:321–331.
Schmahmann JD, Pandya D. (2009) Fiber pathways of the brain. OUP, USA.
Schmahmann JD, Pandya DN, Wang R, Dai G, D'arceuil HE, de Crespigny AJ, Wedeen VJ. 2007. Association fibre pathways of the brain: parallel observations from diffusion spectrum imaging and autoradiography. Brain. 130:630–653.
Schwartz ML, Rakic P, Goldman-Rakic PS. 1991. Early phenotype expression of cortical neurons: evidence that a subclass of migrating neurons have callosal axons. Proc Natl Acad Sci USA. 88:1354–1358.
Shinmyo Y, Terashita Y, Duong TA, Horiike T, Kawasumi M, Hosomichi K, Tajima A, Kawasaki H. 2017. Folding of the cerebral cortex requires cdk5 in upper-layer neurons in gyrencephalic mammals. Cell Rep. 20:2131–2143.
Song JW, Mitchell PD, Kolasinski J, Grant EP, Galaburda AM, Takahashi E. 2015. Asymmetry of white matter pathways in developing human brains. Cereb Cortex. 25:2883–2893.
Srinivasan S, Carlo CN, Stevens CF. 2015. Predicting visual acuity from the structure of visual cortex. Proc Natl Acad Sci USA. 112:7815–7820.
Steele MA. 1998. Tamiasciurus hudsonicus. Mammalian Species. 586:1–9.
Striedter GF. 2005. Principles of brain evolution. Sunderland: Sinauer Assoc.
Striedter GF, Charvet CJ. 2008. Developmental origins of species differences in telencephalon and tectum size: morphometric comparisons between a parakeet (*Melopsittacus undulatus*) and a quail (*Colinus virgianus*). J Comp Neurol. 507:1663–1675. doi:10.1002/cne.21640.
Striedter GF, Srinivasan S, Monuki ES. 2015. Cortical folding: when, where, how, and why? Annu Rev Neurosci. 38:291–307.

Sun T, Hevner RF. 2014. Growth and folding of the mammalian cerebral cortex: from molecules to malformations. Nat Rev Neurosci. 15:217–232. doi:10.1038/nrn3707.

Takahashi E, Dai G, Rosen GD, Wang R, Ohki K, Folkerth RD, Galaburda AM, Wedeen VJ, Ellen Grant P. 2011. Developing neocortex organization and connectivity in cats revealed by direct correlation of diffusion tractography and histology. Cereb Cortex. 21:200–211.

Takahashi E, Dai G, Wang R, Ohki K, Rosen GD, Galaburda AM, Grant PE, Wedeen VJ. 2010. Development of cerebral fiber pathways in cats revealed by diffusion spectrum imaging. Neuroimage. 49:1231–1240. doi:10.1016/j.neuroimage.2009.09.002.

Takahashi E, Folkerth RD, Galaburda AL, Grant PE. 2012. Emerging cerebral connectivity in the human fetal brain: an MR tractography study. Cereb Cortex. 22:455–464.

Takemura H, Caiafa CF, Wandell BA, Pestilli F. 2016. Ensemble tractography. PLoS Comput Biol. 12:e1004692.

Tallinen T, Chung JY, Rousseau F, Girard N, Lefèvre J, Mahadevan L. 2016. On the growth and form of cortical convolutions. Nature Physics. 12:588.

Thomas C, Ye FQ, Irfanoglu MO, Modi P, Saleem KS, Leopold DA, Pierpaoli C. 2014. Anatomical accuracy of brain connections derived from diffusion MRI tractography is inherently limited. Proc Natl Acad Sci. 111:16574–16579.

Toda T, Shinmyo Y, Duong TA, Masuda K, Kawasaki H. 2016. An essential role of SVZ progenitors in cortical folding in gyrencephalic mammals. Sci Rep. 6:29578.

Toro R, Burnod Y. 2005. A morphogenetic model for the development of cortical convolutions. Cereb Cortex. 15:1900–1913.

Tusa RJ, Ungerleider LG. 1985. The inferior longitudinal fasciculus: a reexamination in humans and monkeys. Ann Neurol. 18:583–591.

Usoskin D, Furlan A, Islam S, Abdo H, Lönnerberg P, Lou D, Hjerling-Leffler J, Haeggström J, Kharchenko O, Kharchenko PV, et al. 2015. Unbiased classification of sensory neuron types by large-scale single-cell RNA sequencing. Nat Neurosci. 18:145.

Van Essen DC. 1997. A tension based theory of morphogenesis and compact wiring in the central nervous system. Nature. 385:313–318.

Vogel C, Marcotte EM. 2012. Insights into the regulation of protein abundance from proteomic and transcriptomic analyses. Nat Rev Genet. 13:227–232.

Wedeen VJ, Wang RP, Schmahmann JD, Benner T, Tseng WY, Dai G, Pandya DN, Hagmann P, D'Arceuil H, de Crespigny AJ. 2008. Diffusion spectrum magnetic resonance imaging (DSI) tractography of crossing fibers. Neuroimage. 41: 1267–1277.

Wilber CG, Gilchrist RD. 1965. Organ weight: body weight ratios in the Mongolian gerbil, *Meriones unguiculatus*. Chesapeake Sci. 6:109–114.

Wilkinson M, Lim AR, Cohen AH, Galaburda AM, Takahashi E. 2017. Detection and growth pattern of arcuate fasciculus from newborn to adult. Front Neurosci. 11:389.

Wedeen VJ, Hagmann P, Tseng WY, Reese TG, Weisskoff RM. 2005. Mapping complex tissue architecture with diffusion spectrum magnetic resonance imaging. Magn Reson Med. 54:1377–1386.

Woodward A, Hashikawa T, Maeda M, Kaneko T, Hikishima K, Iriki A, Okano H, Yamaguchi Y. 2018. The Brain/MINDS 3D digital marmoset brain atlas. Sci data. 5:180009.

Workman AD, Charvet CJ, Clancy B, Darlington RB, Finlay BL. 2013. Modeling transformations of neurodevelopmental sequences across mammalian species. J Neurosci. 33:7368–7383.

Wu D, Xu J, McMahon MT, van Zijl PC, Mori S, Northington FJ, Zhang J. 2013. *In vivo* high-resolution diffusion tensor imaging of the mouse brain. Neuroimage. 83:18–26.

Xu G, Knutsen AK, Dikranian K, Kroenke CD, Bayly PV, Taber LA. 2010. Axons pull on the brain, but tension does not drive cortical folding. J Biomech Eng. 132:071013.

Zeng H, Shen EH, Hohmann JG, Oh SW, Bernard A, Royall JJ, Glattfelder KJ, Sunkin SM, Morris JA, Guillozet-Bongaarts AL, et al. 2012. Large-scale cellular-resolution gene profiling in human neocortex reveals species-specific molecular signatures. Cell. 149:483–496.

Zhang D, Guo L, Zhu D, Li K, Li L, Chen H, Zhao Q, Hu X, Liu T. 2013. Diffusion tensor imaging reveals evolution of primate brain architectures. Brain Struct Funct. 218:1429–1450.

Zhang K, Sejnowski TJ. 2000. A universal scaling law between gray matter and white matter of cerebral cortex. Proc Natl Acad Sci USA. 97:5621–5626.

Zilles K, Palomero-Gallagher N, Amunts K. 2013. Development of cortical folding during evolution and ontogeny. Trends Neurosci. 36:275–284.